# Molecular-Shape-Dependent Photophysical Properties of *meso-β* Doubly Linked Zn(II) Porphyrin Arrays and Their Indene-Fused Analogues[†]

**Ji Haeng Heo,[‡] Toshiaki Ikeda,[§] Jong Min Lim,[‡] Naoki Aratani,[§] Atsuhiro Osuka,*[,§] and Dongho Kim*[,‡]**

*Spectroscopy Laboratory for Functional π-Electronic Systems and Department of Chemistry, Yonsei University, Seoul 120-749, Korea, and Department of Chemistry, Graduate School of Science, Kyoto University, Sakyo-ku, Kyoto 606-8502, Japan*

*Received: March 12, 2010; Revised Manuscript Received: April 21, 2010*

*meso-β* doubly linked Zn(II) porphyrin arrays and their indene-fused analogues were prepared by Suzuki−Miyaura coupling and subsequent oxidation with DDQ-$Sc(OTf)_3$. The excited state properties of these conjugated porphyrin arrays have been investigated by steady-state and time-resolved spectroscopy along with quantum mechanical calculations to reveal their molecular shape dependencies with respect to *syn*- versus *anti*-connectivity as well as nonfused versus fused structures. Nonfused *syn*-trimer exhibits nearly the same $S_1$-state lifetime and two-photon absorption (TPA) value as the nonfused dimer, while the nonfused *anti*-trimer exhibits different values. The TD-DFT calculations also demonstrate that the nonfused *anti*-trimer has a different electronic structure from the corresponding *syn*-trimer. Indene-fused dimers and trimers exhibit the enhanced TPA values and shortened $S_1$-state lifetime because of the elongated π-conjugation and the perturbation of electronic structures. Our research provides further insight into the molecular-shape-dependent electronic properties of *meso-β* doubly linked Zn(II) porphyrin arrays.

## I. Introduction

During the past decade, porphyrin molecules have emerged as one of the most desirable building block elements for the fabrication of highly efficient molecular photonic and electronic devices due to their versatile optical and electrochemical properties.[1,2] To realize the mimicries of light harvesting complexes, numerous research activities have been directed toward the design of various types of covalently[3] or noncovalently[4] linked porphyrin arrays. Among them, *meso*−*meso* singly linked and *meso*−*meso*, *β*−*β*, *β*−*β* triply linked porphyrin arrays have been extensively investigated in terms of electronic couplings related with their photophysical properties.[5,6] The former porphyrin arrays exhibit split Soret bands due to the exciton coupling between the adjacent porphyrin units, while their Q-bands remain almost at the same positions. These spectral features indicate that the orthogonal conformation between the neighboring porphyrins disrupts π-electron conjugation, leading to poor π-electron delocalization over the array. On the contrary, the latter porphyrin arrays exhibit drastically red-shifted absorption spectra that reach into the infrared region arising from a reduced HOMO−LUMO energy gap contributed by facile π-electron delocalization along the entire array. These contrasting features in the two types of porphyrin arrays have provided us the prospects as molecular photonic and electronic wires, respectively. Despite these promises, however, triply linked porphyrin arrays have drawbacks of poor solubility, strong aggregation tendency, and chemical instability which become more serious with an increase in the overall molecular length. Therefore, it is important to overcome such limitations for exploitation of fused porphyrin arrays that may serve as molecular electronic wires. In this context, new synthetic attempts have been developed to increase chemical stability, improve solubility, and prevent aggregation phenomena. For instance, doubly strapped porphyrin tapes which have bulky substituents at *meso* positions were prepared to solve these problems.[7] Actually, we could find the absorption spectra which show typical vibrational structures mainly due to the prevention of π−π interaction by the double straps. However, doubly strapped porphyrin tapes are indispensably accompanied by a problem of synthetic difficulties.

Recently, we have synthesized another type of porphyrin arrays in which porphyrin pigments are doubly linked by *meso-β*, *meso-β* positions successfully.[8,9] *meso-β* doubly linked porphyrin arrays show photophysical properties similar to other porphyrin arrays that exhibit red-shifted absorption bands reaching the near-IR region and enhanced two-photon absorption (TPA) cross-section values because of the elongated π-conjugation pathways. Moreover, the aggregation phenomenon induced by π−π interaction was not observed in these arrays, and the lowest Q-like absorption bands tend to remain below 1200 nm, which may be suitable for the practical application with 1240 nm photoexcitation by NIR light sources, especially a commercially available ND:YAG laser. In this regard, the doubly linked porphyrin arrays can be promising candidate molecules for application as molecular electronic wires. Despite their structural advantages, detailed studies on the photophysical properties of doubly linked porphyrin arrays are yet to appear due mainly to the limited synthetic access.

So far, the *meso-β* doubly linked connectivity depends heavily on the $a_{1u}$ HOMO characteristics of metal porphyrins.[8,9] Therefore, there was no synthetic route to *meso-β* doubly linked Zn(II) porphyrin arrays since the cation radical of Zn(II) porphyrin has $a_{2u}$ HOMO. Quite recently, we prepared *meso-β* doubly linked Zn(II) porphyrin arrays via Suzuki−Miyaura coupling reaction between appropriately fabricated borylated

[†] Part of the "Michael R. Wasielewski Festschrift".

* Corresponding authors. E-mail: dongho@yonsei.ac.kr; osuka@kuchem.kyoto-u.ac.jp.

[‡] Yonsei University.

[§] Kyoto University.

10.1021/jp1022696 
Published on Web 05/10/2010

**CHART 1: Schematic Molecular Structures of *meso-β* Doubly Linked Zn(II) Porphyrin Arrays**

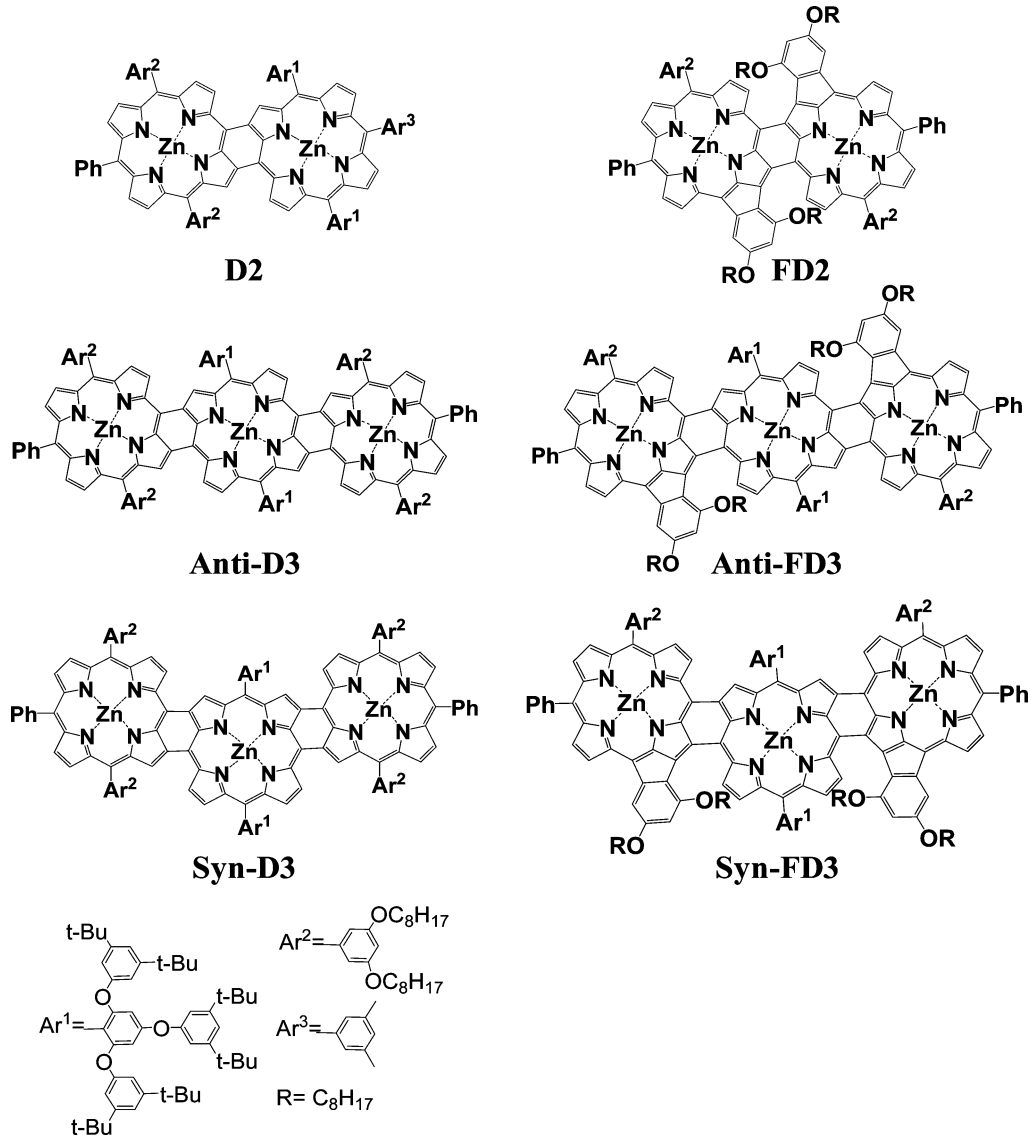


porphyrin and brominated porphyrin and subsequent oxidation with DDQ-Sc(OTf)$_3$.[10] *syn*- and *anti*-isomers of *meso-β* doubly linked Zn(II) porphyrin trimer were separated, which showed distinctly different steady-state absorption and fluorescence spectra, reflecting their molecular shapes in the ($\pi$,$\pi$*) electronic transitions.[10] This feature implies that each isomer has unique electronic structure depending on its molecular shape. Thus, it is relevant to investigate the molecular-shape-dependent photophysical properties of doubly linked porphyrin arrays. In the course of these studies, we have found that the oxidation of *meso-β* singly linked Zn(II) diporphyrin under stronger conditions led to the formation of an indene-fused analogue (Chart 1).

In this work, we have utilized various spectroscopic techniques such as femtosecond transient absorption and femtosecond Z-scan measurements along with quantum mechanical calculations to explore the influences of molecular connectivity (*syn*- versus *anti*-) and fused structure (nonfused versus fused) upon the photophysical properties of *meso-β* doubly linked Zn(II) porphyrin arrays. On the basis of these measurements, we have observed the difference in the electronic structures of *meso-β* doubly linked Zn(II) porphyrin arrays depending on their molecular shapes.

## II. Experimental Section

**Sample Preparation and Steady-State Absorption.** *meso-β* doubly linked Zn(II) porphyrin arrays were prepared according to the reported methods.[10]

Toluene (spectroscopic grade, ≥99.5% purity) solvent was purchased from Sigma-Aldrich and used without further purification. UV−vis absorption spectra were recorded with a Cary-5000 UV−vis−NIR spectrometer. A quartz cell with an optical path length of 10 mm was used for all of the steady-state absorption measurements.

**Femtosecond Z-Scan Method.** The TPA measurements were performed using the open-aperture Z-scan method with 130 fs pulses from an optical parametric amplifier (Light Conversion, TOPAS) operating at a 2 kHz repetition rate using a Ti:sapphire regenerative amplifier system (Spectra-Physics, Hurricane X). After passing through an $f = 10$ cm lens, the laser beam was focused to a 1 mm quartz cell. As the position of the sample cell was varied along the laser-beam direction ($z$-axis), the transmitted laser beam from the sample cell was then probed using a Ge/PN photodiode (New Focus, 2033) as used for reference monitoring. Assuming a Gaussian beam profile, the nonlinear absorption coefficient $\beta$ can be obtained by curve

fitting to the observed open aperture traces with the following equation[11]

$$T(z) = 1 - \frac{\beta I_0(1 - e^{-\alpha_0 l})}{2\alpha_0(1 + (z/z_0)^2)}$$

where $\alpha_0$ is a linear absorption coefficient; $I_0$ is the on-axis peak intensity of the incident pulses at the focal point; $l$ is a sample length; and $z_0$ is the diffraction length of the incident beam. After obtaining the nonlinear absorption coefficient $\beta$, the TPA cross-section $\sigma^{(2)}$ (in units of 1 GM = $10^{-50}$ cm$^4$•s•photon$^{-1}$molecule$^{-1}$) of a single solute molecule can be determined by using the following relationship

$$\beta = \frac{\sigma^{(2)} N_A d \times 10^{-3}}{h\upsilon}$$

where $N_A$ is the Avogadro constant; $d$ is the concentration of the TPA compound in solution; $h$ is Planck's constant; and $\upsilon$ is the frequency of the incident laser beam. The TPA cross-section value of AF-50 was measured as a reference compound, which was found to exhibit a TPA value of 50 GM at 800 nm.[12]

**Femtosecond Transient Absorption.** The femtosecond time-resolved transient absorption (TA) spectrometer pumped by a Ti:sapphire regenerative amplifier system (Quantronix, Integra-C) operating at 1 kHz repetition rate and an optical detection system. The frequency doubled 400 nm pulses had a pulse width of ~100 fs and an average power of 1 mW which were used as pump pulses. White light continuum (WLC) probe pulses were generated using a sapphire window (2 mm of thickness) by focusing a small portion of the fundamental 800 nm pulses. The time delay between pump and probe beams was carefully controlled by making the pump beam travel along a variable optical delay (Newport, ILS250). Intensities of the spectrally dispersed WLC probe pulses are monitored by a miniature spectrograph (OceanOptics, USB2000+). To obtain the time-resolved transient absorption difference signal ($\Delta A$) at a specific time, the pump pulses were chopped at 25 Hz, and absorption spectra intensities were saved alternately with or without pump pulse. Typically, 6000 pulses excite samples to obtain the TA spectra at a particular delay time. The polarization angle between the pump and probe beam was set at the magic angle (54.7°) to prevent polarization-dependent signals. Cross-correlation fwhm in pump−probe experiments was less than 200 fs, and chirp of WLC probe pulses was measured to be 800 fs in the 400−800 nm region. To minimize chirp, all reflection optics in the probe beam path and 2 mm path length of the quartz cell were used. The three-dimensional data sets of $\Delta A$ versus time and wavelength were subjected to singular value decomposition and global fitting to obtain the kinetic time constants and their associated spectra using Surface Xplorer software.[13]

For the transient absorption anisotropy decay ($r(t)$) measurements, the probe white-light continuum pulse was set to have vertical polarization. The excitation pulse then was changed to have parallel or perpendicular polarization by rotating a half wave plate centered at 400 nm, with respect to the polarization of the probe pulse. Finally, the transient absorption anisotropy decay can be obtained by the following equation

$$r(t) = (I_{ll} - I_{\perp})/(I_{ll} + 2I_{\perp})$$

where the variable represents amplitude.

**Computational Methods.** Quantum mechanical calculations were performed with the Gaussian 03 program suite.[14] All calculations were carried out using the density functional theory (DFT) method employing the B3LYP functional as the 6-31G(d) basis set for all of the atoms. The X-ray crystal structures were used as initial geometry for geometry optimization. To simulate the ground state absorption spectra, we used the time-dependent density functional theory (TD-DFT) method using the same functional and basis set as those used for geometry optimization.

## III. Results

**Synthesis of *meso*-$\beta$ Doubly Linked Zn(II) Porphyrin Arrays.** *meso*-$\beta$ doubly linked Zn(II) porphyrin arrays **D2**, **Anti-D3**, and **Syn-D3** were synthesized from *meso*-$\beta$ singly linked Zn(II) porphyrin arrays **S2**, **Anti-S3**, and **Syn-S3** according to the reported method.[10] Oxidation of **S2**, **Anti-S3**, and **Syn-S3** by an excess amount of DDQ and $Sc(OTf)_3$ at 80 °C for 2 h afforded **FD2**, **Anti-FD3**, and **Syn-FD3**, respectively (Supporting Information, Scheme S1). These compounds were characterized by $^1$H NMR and MALDI-TOF mass spectroscopies (see Supporting Information). In the $^1$H NMR spectrum, **FD2** showed three mutually coupled doublets for the $\beta$-protons without singlet for the $\beta$-proton, indicating that the $\beta$-proton responsible for the singlet signal in **D2** disappeared in **FD2**. Furthermore, only five peaks were observed for the Ar$^2$ protons, indicating that fusion reaction occurred between the $\beta$-position of porphyrin and the *o*-position of Ar$^2$. In addition to these observations, broad peaks corresponding to the octyloxy protons were observed around −0.5−0.5 ppm. This upfield shift indicates that the octyloxy chain is located just above the porphyrin ring, in line with the assigned indene-fused structure. It is conceivable that **FD2** is forced to take a twisted conformation due to the steric repulsion between the fused ring and porphyrinic $\beta$-hydrogen atom. For this reason, **FD2** can take two atropisomers, *meso* form and *dl* form. Fortunately, the identification of these atropisomers has been accomplished by single-crystal X-ray diffraction analysis (Figure 1).[15] Phenyl substituents are doubly fused at the $\beta$-position to form an indene skeleton and are distorted toward the same side from the porphyrin coplanar plane to take *dl* form. In the solid structure, the dihedral angle between two porphyrin planes is 32.3°.

Such identification of the atropisomers has also been difficult for **Anti-FD3**. In the case of **Syn-FD3**, the $^1$H NMR showed four peaks for the Ar$^1$-*meta*-protons, indicating that each fused phenyl ring is distorted toward the same side. Namely, the isolated **Syn-FD3** has *syn*-stereochemistry also for the fusion direction.

**Steady-State Absorption Spectra.** Figure 2 shows the steady-state absorption spectra of *meso*-$\beta$ doubly linked Zn(II) porphyrin arrays and indene-fused *meso*-$\beta$ doubly linked Zn(II) porphyrin arrays in toluene, which are normalized at the high-energy Soret bands. The absorption bands are roughly categorized into three distinct well-separated subgroups, which are marked as band I, II, and III, respectively.

The absorption spectra of doubly linked Zn(II) porphyrin arrays are similar to those of *meso*−*meso*, $\beta$−$\beta$, $\beta$−$\beta$ triply linked arrays; the distinct bands I and II arise from the Soret band of a monomer, while the band III originates from the monomer's Q-band. With an increase in the overall molecular length, the band I remains at nearly the same positions, but the bands II and III are continuously red-shifted and intensified.

Interestingly, even though the absorption band positions of **Anti-D3** and **Syn-D3** are almost the same, the absorption spectra become broader with more split spectral shapes, especially in

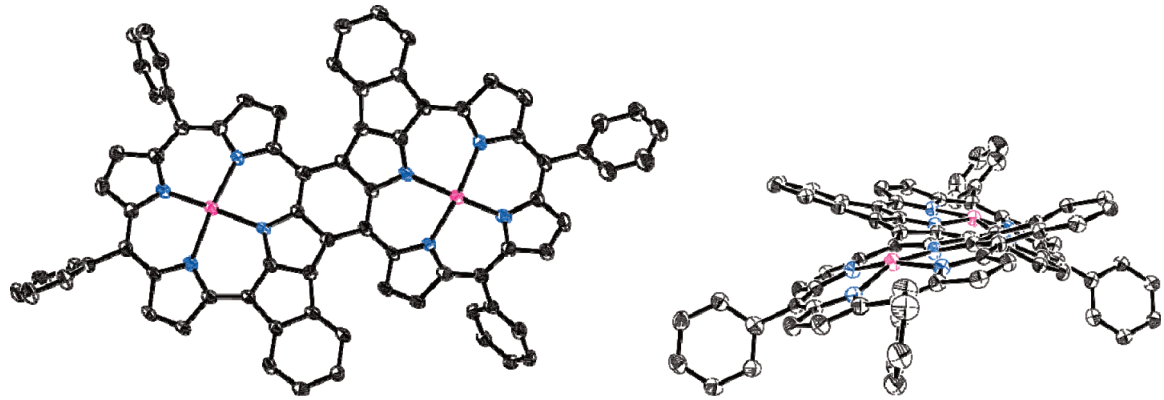

**Figure 1.** X-ray crystal structure of **FD2**. Top view (left) and side view (right). Octyloxy groups, hydrogen atoms, and solvent molecules are omitted for clarity. The ellipsoids are scaled to the 50% probability level.

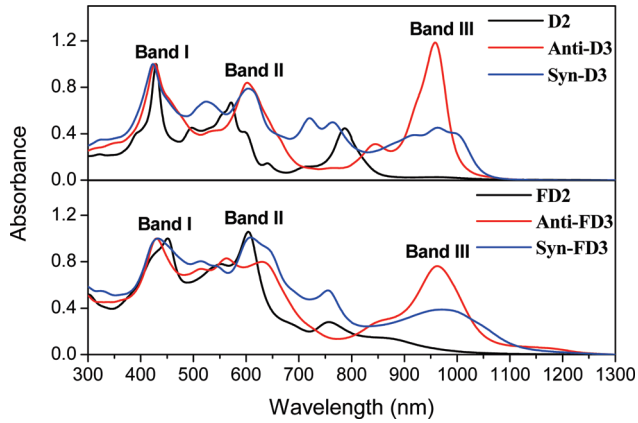


**Figure 2.** Steady-state absorption spectra of doubly linked Zn(II) porphyrin arrays in toluene.

**Syn-D3**. In this regard, it is worthwhile to point out that a geometrical change induces electronic perturbation in **Syn-D3**. Furthermore, especially at band III, while **Anti-D3** shows a narrow and intensified absorption peak, **Syn-D3** shows a diminished and featureless absorption band, indicating that each trimer has different electronic structure.

In the indene-fused doubly linked arrays, the absorption bands are red-shifted compared with nonfused doubly linked arrays mainly due to the elongation of $\pi$-conjugation pathways. Additionally, the indene-fused doubly linked arrays exhibit broader absorption spectra than the nonfused doubly linked arrays, which may arise from the increased steric repulsion in indene-fused doubly linked arrays (Supporting Information, Figures S2 and S3). Similar to the nonfused doubly linked arrays, while **Anti-FD3** shows an intensified absorption band III, **Syn-FD3** exhibits a broad and diminished absorption band III.

**Transient Absorption Measurements.** To explore the excited state dynamics of doubly linked Zn(II) porphyrin arrays, we have carried out femtosecond transient absorption measurements. In our previous studies on the triply linked Zn(II) porphyrin arrays, we observed that the $S_1$-state lifetimes are systematically decreased with an increase in the number of porphyrins mainly due to the acceleration of nonradiative relaxation processes caused by the reduced HOMO−LUMO energy gaps.[6c] For doubly linked Ni(II) porphyrin arrays, however, the $S_1$-state lifetimes become longer as the number of porphyrin moieties increases because various charge transfer and (d,d) states caused by central $d^8$ Ni(II) ion exist below the ($\pi$,$\pi$*) states of the porphyrin macrocycle.[9] As a consequence, the observed decay times in doubly linked Ni(II) porphyrin arrays should not correspond to the excited $S_1$ ($\pi$,$\pi$*) state lifetimes.

In our current molecular systems, as the porphyrin macrocycle is metalated by closed-shell Zn(II), the $S_1$ ($\pi$,$\pi$*) state dynamics is not affected by a central metal ion, thus we can examine the singlet excited state dynamics contributed by porphyrin ($\pi$,$\pi$*) states. The transient absorption spectra of the *meso-β* doubly linked Zn(II) porphyrin arrays were measured after photoexcitation at 800 nm. All the transient absorption spectra exhibit strong ground state bleaching (GSB) recovery corresponding to their ground state absorption bands and broad excited state absorption (ESA) signals covering the whole visible region (Figures 3 and 4). The temporal profiles of femtosecond transient absorption changes show ultrafast energy relaxation processes occurring within a few tens of picosecond time scale. Similar to other porphyrin arrays, as the number of porphyrin units increases, the lowest excited state lifetimes become shorter. The lowest excited state lifetimes for **D2**, **Anti-D3**, and **Syn-D3** were measured to be 19.2, 14.7, and 19 ps, respectively. It is noteworthy that the lifetime of **Syn-D3** is different from that of **Anti-D3**, which is almost the same as that of **D2**. From these results, we can suppose that the $S_1$-state dynamics of *meso-β* doubly linked porphyrin trimers are associated with their molecular shapes.

The $S_1$-state lifetimes for the indene-fused doubly linked arrays were also measured under the same experimental conditions (insets, Figure 4). The excited state decay dynamics for **FD2**, **Anti-FD3**, and **Syn-FD3** show double exponential decays with the short time constant of 2.5 ps in common and the second decay time constants of 10.5, 8.4, and 10.3 ps, respectively. Overall, the $S_1$-state lifetimes of the fused doubly linked porphyrin arrays are shorter than those of nonfused ones probably because the energy gaps between the HOMO and LUMO levels are reduced by the elongated $\pi$-conjugation pathways as demonstrated in the absorption spectra. In addition, the increased geometrical steric repulsion between porphyrin moieties in indene-fused doubly linked arrays seems to accelerate the nonradiative relaxation processes, leading to shorter excited state lifetimes.

Of interest here is the fact that the lifetimes of *syn*-type trimers are almost the same as those of dimers in both nonfused and fused doubly linked arrays. This feature indicates that the $S_1$-state dynamics of doubly linked Zn(II) porphyrin arrays are governed by the molecular shape as well as the elongated $\pi$-conjugation pathway.

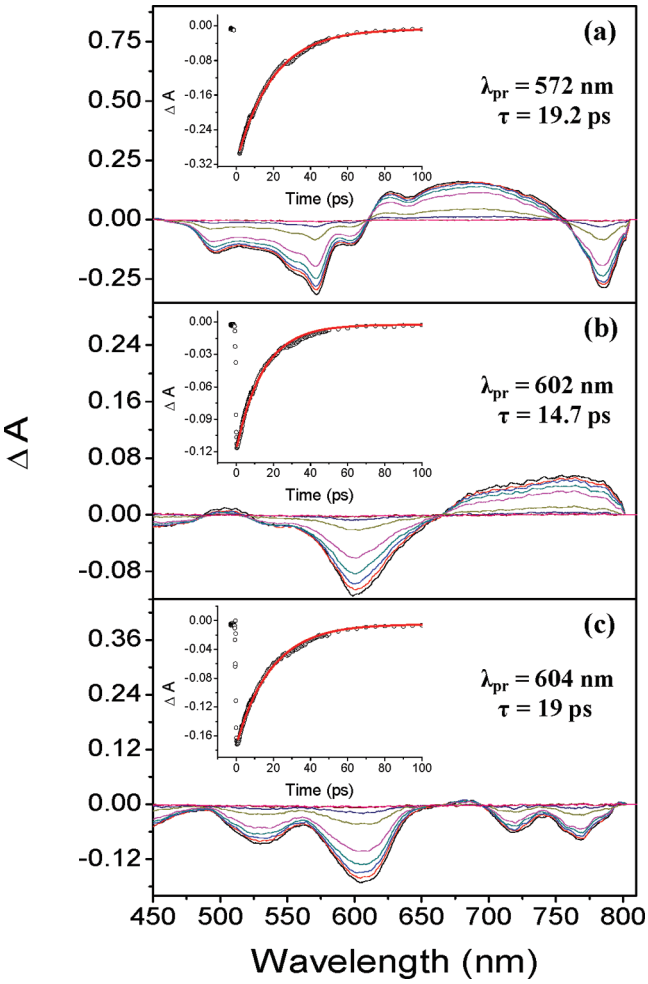


**Figure 3.** Transient absorption spectra of (a) **D2**, (b) **Anti-D3**, and (c) **Syn-D3** in toluene after photoexcitation at 800 nm at several time delays. Inset shows the transient absorption decay profiles for ground state bleaching.

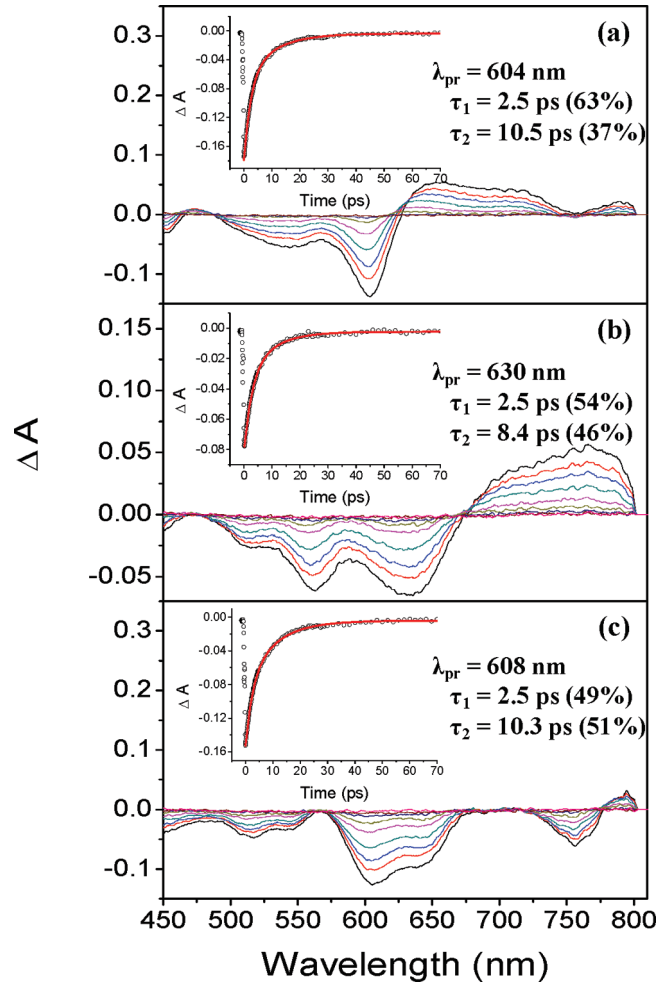


**Figure 4.** Transient absorption spectra of (a) **FD2**, (b) **Anti-FD3**, and (c) **Syn-FD3** in toluene after photoexcitation at 800 nm at several time delays. Inset shows the transient absorption decay profiles for ground state bleaching.

**Measurement of TPA Cross-Section Values.** The two-photon absorption cross-section values of doubly linked Zn(II) porphyrin arrays were measured by using an open-aperture Z-scan method upon exciting the molecule with NIR femtosecond optical pulses. We have selected two-photon excitation wavelengths for the TPA measurements to avoid any contribution from one-photon transition.

The TPA cross-section values for **D2**, **Anti-D3**, and **Syn-D3** were measured to be 7000, 17600, and 8700 GM, respectively (Supporting Information, Figures S4 and S5 and Table 1). As demonstrated for other porphyrin array systems, it is well-established that the TPA values are strongly related with the effective $\pi$-conjugation lengths.[16] However, it is of interest to note that the TPA cross-section value of **Anti-D3** has reached 17600 GM, more than twice the value of its *syn*-array **Syn-D3**, indicating that the molecular shape as well as the $\pi$-conjugation length is an important parameter in the enhancement of TPA values.

While **Anti-D3** has an increased TPA value larger than twice that of its dimer by efficient $\pi$-electron conjugation through linearly linked porphyrin arrays, restricted $\pi$-electron delocalization due to the bent structure in **Syn-D3** gives rise to a relatively small TPA value. Furthermore, it should be noted that the TPA value of **Syn-D3** is similar to that of **D2**. On the basis of the excited state dynamics and TPA values, we know that the *syn*-trimer shows a photophysical behavior similar to the dimer. The TPA cross-section values of **D2** and **Anti-D3** are comparable to those of corresponding Ni(II) porphyrin arrays,[9] implying that the effect by central metal ions on the TPA properties seems to be negligible in *meso*-$\beta$ doubly linked porphyrin arrays.

Similarly, the TPA cross-section values of **FD2**, **Anti-FD3**, and **Syn-FD3** were measured to be 11600, 23600, and 17100 GM, respectively. The larger TPA cross-section values for the fused doubly linked arrays than the nonfused arrays arise from the enhanced polarizability due to the elongation of $\pi$-electron delocalization throughout the fused indene rings. In this case, it should be mentioned that the TPA value of **Syn-FD3** is not equal to that of **FD2**, reflecting that the indene ring fusion strongly influences the TPA values.

## IV. Discussion

**Electronic Structures Depending on Molecular Shapes.** On the basis of our experimental results, we have confirmed the unique photophysical properties of *meso*-$\beta$ doubly linked Zn(II) porphyrin arrays depending on their molecular shapes. To explore the effect of molecular shapes on the electronic structures, we have adopted the quantum-mechanical calculations. First of all, the vertical excitation energies were calculated by using time-dependent density functional theory (TD-DFT) to simulate the ground state absorption spectra (Figure 5). In

**TABLE 1: Summary of Results from Steady-State, Quantum Mechanical Calculation, and Time-Resolved Measurements**

| molecules | absorption band I | absorption band II | absorption band III | dihedral angle (deg) | $\sigma^{(2)}$ (GM) ($\lambda_{ex}$/nm)[d] | $\tau_s$ (ps)[e] |
|---|---|---|---|---|---|---|
| **D2** | 429 | 572 | 787 | 26.8 | 7000 (1500) | 19.2 |
| **Anti-D3** | 427 | 602 | 958 | 24.1[a], 22.8[b], 2.4[c] | 17600 (1900) | 14.7 |
| **Syn-D3** | 423 | 604 | 963 | 22.2, 22.2, 28.9 | 8700 (1900) | 19 |
| **FD2** | 451 | 604 | 870 | 31.1 | 11600 (1450) | 2.5, 10.5 |
| **Anti-FD3** | 430 | 630 | 963 | 26.5, 26.5,0 | 23600 (1850) | 2.5, 8.4 |
| **Syn-FD3** | 432 | 608 | 970 | 27.8, 27.9, 52.3 | 17100 (1900) | 2.5, 10.3 |

[a] Angle between two normal vectors of the mean planes of the first porphyrin and second porphyrin. [b] The second porphyrin and terminal porphyrin. [c] The first porphyrin and terminal porphyrin. [d] $\lambda_{ex}$ is the laser excitation wavelength. [e] $S_1$-state lifetime in maximum ground state bleaching.

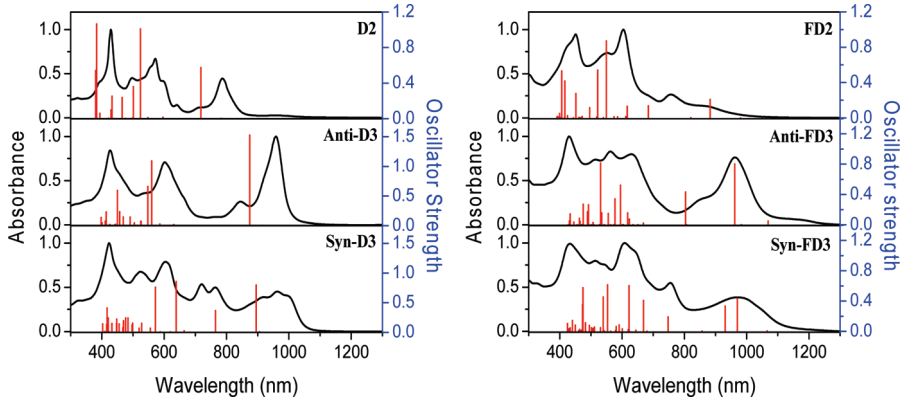


**Figure 5.** Vertical excitation data calculated by using TD-DFT (red) and ground state absorption spectra (black) for doubly linked Zn(II) porphyrin arrays.

all molecules, the calculated transitions are well matched with the experimental absorption spectra in the positions and intensities of absorption bands.

In **D2**, the transition dipole moment is parallel to the long molecular *x*-axis for the bands II and III. On the contrary, the transition dipole moment for band I is aligned along the short molecular *y*-axis, which is perpendicular to the long molecular *x*-axis. In the absorption spectra, as one porphyrin unit is additionally linked linearly at **D2**, the band I remains at the same position; however, the bands II and III are red-shifted and intensified. Compared with **Anti-D3**, **Syn-D3** which is formed by a nonlinear porphyrin linkage to **D2** shows the same position in their absorption bands but exhibits broader absorption bands and especially decreased absorption band III. From the TD-DFT calculations, with an increase in the overall molecular length, the long *x*-axis transition dipole moment is linearly enhanced for **Anti-D3** (the calculated absorption peak is presented at 874 nm, and the corresponding oscillator strength is 0.8). Because of efficient $\pi$-conjugation along the *x*-axis, the relevant transition dipole moment is significantly enhanced for band III, hence intensifying the absorption band. On the other hand, **Syn-D3** exhibits a broad absorption feature at band III, and in the TD-DFT calculations, we can find two *x*-axis transition dipoles (764 and 895 nm, respectively), which have smaller oscillator strengths. Accordingly, it is assumed that band III is composed of two distinct long *x*-axis transition dipoles.

To explain the shape-dependent photophysical properties observed in the steady-state absorption spectra, we have introduced a schematic molecular model (Scheme 1). As shown in Scheme 1, the red arrows are *y*-axis transition dipole moments and the blue ones *x*-axis transition dipole moments, respectively. **D2** has two components with *x*-axis and *y*-axis transitions which are perpendicular to each other. As the number of porphyrin moieties increases, the *x*-axis transition dipole is increased

**SCHEME 1: Schematic Diagram of Transition Dipole Moment of *meso-β* Doubly Linked Zn(II) Porphyrin Arrays**

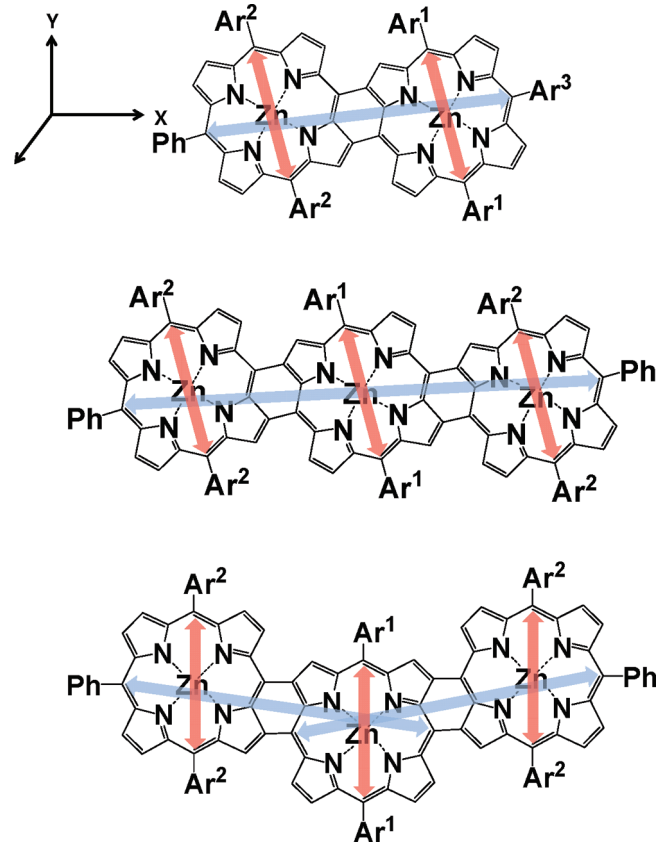


linearly in **Anti-D3.** On the other hand, **Syn-D3** is formed by a bent linkage of porphyrin units, and as a consequence, the

direction of the *x*-axis transition dipole is different from that of **Anti-D3**. Accordingly, we think that **Syn-D3** behaves like two independent porphyrin dimer units. This assumption is clearly illustrated by the TD-DFT calculations in that the two separated *x*-axis transition dipoles in the *syn*-trimer are presented in the calculated absorption spectra with smaller oscillator strengths than the *anti*-trimer. Since two distinct transition dipoles are not fully overlapped, we can consider that the *syn*-trimer is composed of two separated porphyrin dimer units. For this reason, *meso*-$\beta$ doubly linked porphyrin trimers have unique electronic structures depending on molecular shapes.

In the indene-fused doubly linked array systems, the vertical excitation data show more complicated transition dipoles than those of nonfused arrays, which is consistent with the red-shifted and more split absorption spectra of the fused doubly linked arrays. The elongation of $\pi$-conjugation pathways as well as electronic perturbation caused by enhanced steric repulsion represents that the absorption bands of indene-fused doubly linked arrays are broader than those of nonfused arrays. Furthermore, the fused benzene ring attached to the porphyrin unit enhances the *y*-axis transition dipole, and as a consequence, the band II becomes more intensified and the overall absorption spectra show complicated features. In addition, the fused doubly linked porphyrin trimers also show different electronic transitions depending on molecular shapes, indicating that a model for two separated *x*-axis transition dipoles is appropriate in explaining the electronic structures of the fused porphyrin trimers.

On the basis of time-resolved spectroscopic results, we can also demonstrate that the two- dimer model is reasonable to explain the molecular-shape-dependent properties in the doubly linked porphyrin arrays. The $S_1$-state lifetimes of nonfused doubly linked arrays measured by using the femtosecond transient absorption technique were found to be ~20 ps. As the number of porphyrin units increases, the $S_1$-state lifetime becomes shorter. Actually, we could observe that the $S_1$-state lifetime of **Anti-D3** is shorter than that of **D2**. However, in the case of **Syn-D3**, the $S_1$-state lifetime is similar to **D2**, supporting the fact that the *syn*-trimer is composed of two independent porphyrin dimer units. Likewise, in the fused doubly linked porphyrin arrays, the *syn*-trimer exhibits nearly the same lifetime as the dimer. Accordingly, from this experimental evidence, it is clear that the *syn*-trimer is separated into the two independent dimer units.

Interestingly, the TPA value of **Syn-D3** is similar to that of **D2**, representing the same feature as the $S_1$-state lifetime measurements. It means that in spite of the increased overall molecular length the polarizability of **Syn-D3** is not increased significantly, and as a consequence, **Syn-D3** has smaller TPA values than that of **Anti-D3**. In other words, nonlinear porphyrin linkage to **D2** does not increase significantly the polarizability of **Syn-D3**, and thus **Syn-D3** nearly behaves as **D2**.

**Ring Fusion Effect on Electronic Structures.** According to the two independent dimer models introduced in the previous section, it was supposed that the *anti*-trimer and *syn*-trimer have electronic structures different from each other, and the *syn*-trimer exhibits photophysical properties similar to the dimer. In addition to this result, we have also observed the interesting experimental results by introducing indene ring fusion. First of all, it is noteworthy that an indene ring fusion strongly influences the TPA values. Unlike the corresponding nonfused *syn*-trimer, the indene-fused *syn*-trimer, **Syn-FD3**, has reached the TPA value of 17100 GM which is larger than that of dimer, **FD2**. To investigate another effect on the TPA values in terms of indene ring fusion as well as molecular shape, we have performed frontier molecular orbital (MO) calculations. For **Anti-D3** and **Syn-D3**, the HOMO−LUMO energy gap is quite similar (1.63 and 1.69 eV, respectively), while the shape of each MO density becomes slightly different. That is, **Syn-D3** has a partially localized molecular orbital density, especially at the LUMO+1 and LUMO+2 levels through the array; however, in **Anti-D3**, the MO density is delocalized over the whole array (Supporting Information, Figure S6). In two-photon absorption spectra, the maximum peak was observed in the band III region. From the TD-DFT calculations, we found that the HOMO → LUMO transition and other minor ones give rise to the lowest singlet excited state. For example, the HOMO−1 → LUMO transition contributes to the $S_1$-state of **Anti-D3**, and the HOMO−1 → LUMO+1 transition contributes to the $S_1$-state of **Syn-D3**. Because the two-photon absorption phenomenon, third-order nonlinear optical property, is well-known to be sensitive to $\pi$-electron delocalization, **Syn-D3** exhibiting two-photon absorption transition to the partially localized LUMO+1 level has smaller TPA values, but **Anti-D3** has a relatively larger TPA value due to the TPA transition to the delocalized MO level. However, the relative transitions contributing to the $S_1$-state have a very small contribution (~6%) compared with the HOMO−LUMO transition. Accordingly, the two independent dimer model is quite relevant to explain the TPA results for nonfused doubly linked porphyrin arrays.

The overall MO densities of the fused doubly linked arrays are similar to their corresponding nonfused arrays. However, since the ring fusion induces $\pi$-conjugation elongation, the expanded MO densities at the fused ring sites are observed especially at the HOMO−2 level (Supporting Information, Figure S7). The TD-DFT calculations of **Syn-FD3** indicate that the HOMO → LUMO (59%) and HOMO−2 → LUMO transitions (27%) contribute to the $S_1$-state of **Syn-FD3**. Actually, the HOMO−2 → LUMO transition has a large contribution to the $S_1$-state, indicating that the ring fusion highly influences the TPA values. Consequently, although the *syn*-trimer behaves as the dimer, the ring fusion affects more significantly the TPA values compared with the dimer, and thus the *syn*-trimer exhibits larger TPA value than that of the dimer in the fused doubly linked porphyrin arrays.

As mentioned above, the short decay component with a 2.5 ps time constant was observed in the transient absorption decay profiles of indene-fused doubly linked arrays. One possible explanation for this fast decay component is a dephasing dynamics between the two transition dipole moments. Actually, the fused indene ring might enhance the *y*-axis transition dipole which gives rise to a perturbation of dephasing dynamics between the two transition dipole moments. To confirm this possibility, the femtosecond transient absorption anisotropy (TAA) measurements were performed. Upon excitation with polarized light, however, we could not find evidence on ultrafast dephasing dynamics between the two transition dipole moments.

As another possibility, the vibrational relaxation process can be assigned to this process. Actually, we can observe the broad absorption spectra in the band III region along with the absorption tail in the fused doubly linked arrays, while such an absorption tail was not observed in the corresponding nonfused doubly linked arrays. If we regard this absorption tail as aggregation phenomena due to their self-assembling nature by $\pi-\pi$ stacking, the absorption tail should disappear with a spectral narrowing when *n*-butylamine is added to the sample solution. However, the absorption spectra of the fused doubly linked arrays do not exhibit such absorption spectral changes

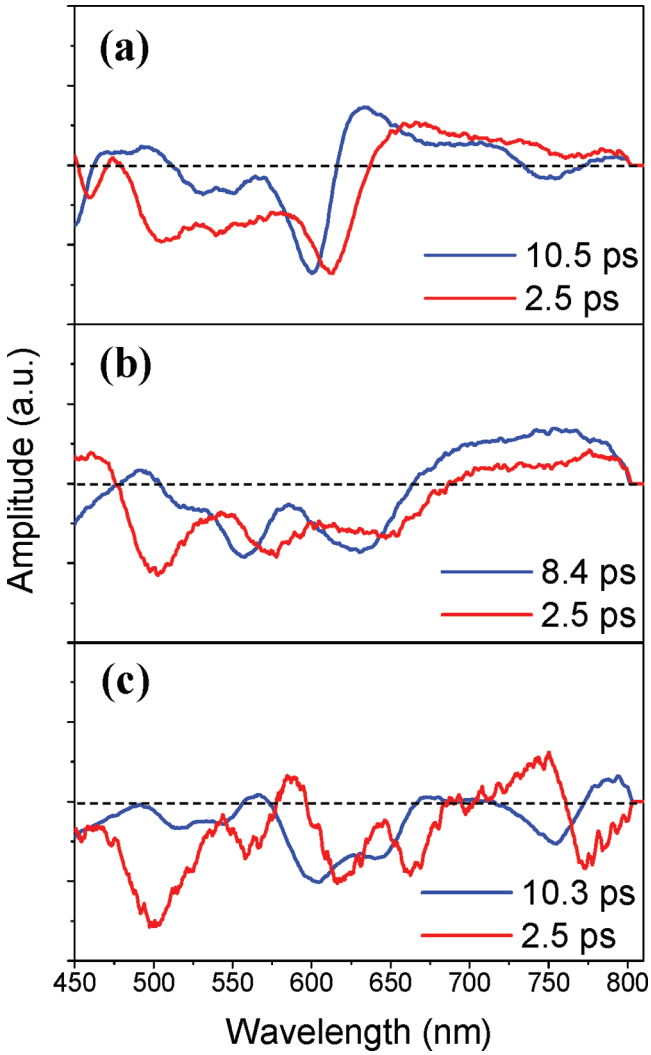


**Figure 6.** Decay associated difference spectra of (a) **FD2**, (b) **Anti-FD3**, and (c) **Syn-FD3** obtained from a global fitting analysis.

(Supporting Information, Figure S8), indicating the electronic transition corresponds to the lowest excited state. Although this transition has extremely small oscillator strength, the existence of such an excited state suggests a possibility of the vibrational relaxation processes. The evidence on the vibrational relaxation process can be seen in the transient absorption spectra. In the fused arrays, the transient absorption spectra show a slightly blue-shifted GSB and ESA band in the whole visible region (Figure 4), while the corresponding TA spectra of nonfused arrays do not exhibit such a band shift. This feature is clearly revealed by decay associated difference spectra (DADS) which shows the spectral profiles of the kinetic components obtained from the global fitting analysis, where the two-components best fit reveals the amplitude spectra corresponding to the two time constants. As shown in the global fitting analysis as depicted in Figure 6, the transient absorption spectra of the 2.5 ps decay component is located at the red-shifted region as compared with that of the longer time component. That is, after photoexcitation, the excited state population relaxes to the lowest $S_1^0$-state in 2.5 ps and then decays to the ground state within ~10 ps. Consequently, we can conclude that the ultrafast relaxation component with the time constant of 2.5 ps originates from the vibrational relaxation dynamics in the fused doubly linked arrays.

## V. Conclusions

In this work, we synthesized the indene-fused *meso-β* doubly linked Zn(II) porphyrin arrays by DDQ-SC(OTf)$_3$ oxidation under strong conditions. We have comparatively studied unique photophysical properties of doubly linked Zn(II) porphyrin arrays depending on their molecular shapes. Doubly linked Zn(II) porphyrin trimer can be divided into two isomers, **Anti-D3** and **Syn-D3**, respectively. While **D2** and **Anti-D3** show absorption spectral features similar to other porphyrin arrays, **Syn-D3** shows different absorption spectra. Since the TD-DFT calculations reveal that clearly separated two *x*-axis transition dipoles are not overlapped in the *syn*-porphyrin array, we can consider that the *syn*-trimer is composed of the two independent porphyrin dimer units. From the time-resolved spectroscopic measurements, the *syn*-trimer shows $S_1$-state lifetime and TPA cross-section value similar to the doubly linked porphyrin dimer. In this context, the two dimer model is acceptable to explain the shape-dependent photophysical properties observed in the *syn*-doubly linked Zn(II) porphyrin trimer.

The fusion of an indene moiety at the porphyrin unit causes steric repulsion and elongated $\pi$-conjugation, leading to a decreased HOMO−LUMO energy gap. These features give rise to enhanced TPA cross-section values as well as shortened $S_1$-state lifetime compared with nonfused doubly linked porphyrin arrays. Consequently, since *meso-β* doubly linked Zn(II) porphyrin arrays exhibit different photophysical properties depending on their molecular shape as well as the fused structure, this strategy will be further utilized for the development of specific molecular photonic devices.

**Acknowledgment.** The work at Yonsei University was supported by the Star Faculty and World Class University (R32-2008-000-10217-0) Programs from the Ministry of Education, Science, and Technology (MEST) of Korea and the AFSOR/AOARD Grant (FA2386-09-1-4092). The quantum calculations were performed using the supercomputing resources of the Korea Institute of Science and Technology Information (KISTI). The work at Kyoto University was supported by Grants-in-Aid for Scientific Research from MEXT (No. 19205006 (A) and 20108001 "pi-Space"). T.I. thanks the JSPS Fellowship for a Young Scientist.

**Supporting Information Available:** Details of sample preparation, $^1$H NMR spectra, optimized molecular structures, open-aperture femtosecond Z-scan data, frontier MO diagrams, and absorption spectra of indene-fused arrays containing 1% *n*-butylamine. This material is available free of charge via the Internet at http://pubs.acs.org.

## References and Notes

(1) (a) Szacilowski, K.; Macyk, W.; Drzewiecka-Matuszek, A.; Brindell, M.; Stochel, G. *Chem. Rev.* **2005**, *105*, 2647. (b) Odobel, F.; Fortage, J. C. R. *Chimie* **2009**, *12*, 437. (c) Holten, D.; Bocian, D. F.; Lindsey, J. S. *Acc. Chem. Res.* **2002**, *35*, 57.

(2) (a) Fujitsuka, M.; Hara, M.; Tojo, S.; Okada, A.; Troiani, V.; Solladie, N.; Majima, T. *J. Phys. Chem. B* **2005**, *109*, 33. (b) Kim, D.; Osuka, A. *Acc. Chem. Res.* **2004**, *37*, 735. (c) Cho, S.; Li, W.-S.; Yoon, M.-C.; Ahn, T. K.; Jiang, D.-L.; Kim, J.; Aida, T.; Kim, D. *Chem.—Eur. J.* **2006**, *12*, 7676. (d) Takahashi, R.; Kobuke, Y. *J. Org. Chem.* **2005**, *70*, 2745. (e) Hasobe, T.; Kamat, P. V.; Absalom, M. A.; Kashiwagi, Y.; Sly, J.; Crossley, M. J.; Hasomizu, K.; Imahori, H.; Fukuzumi, S. *J. Phys. Chem. B* **2004**, *108*, 12865. (f) Ayabe, M.; Ikeda, A.; Kubo, Y.; Takeuchi, M.; Shinkai, S. *Angew. Chem., Int. Ed.* **2002**, *41*, 2790.

(3) (a) Hori, T.; Nakamura, Y.; Aratani, N.; Osuka, A. *J. Organomet. Chem.* **2007**, *692*, 148. (b) Anderson, A.; Anderson, H. L.; Sanders, J. K. M. *Angew. Chem., Int. Ed.* **1992**, *31*, 907. (c) Sugiura, K.; Fujimoto, Y.; Sakata, Y. *Chem. Commun.* **2000**, 1105. (d) Hwang, I.-W.; Aratani, N.; Osuka, A.;

Kim, D. *Bull. Korean Chem. Soc.* **2005**, *26*, 19. (e) Morandeira, A.; Vauthey, E.; Schuwey, A.; Gossauer, A. *J. Phys. Chem. A* **2004**, *108*, 5741.

(4) (a) Hajjaj, F.; Yoon, Z. S.; Yoon, M.-C.; Park, J.; Satake, A.; Kim, D.; Kobuke, Y. *J. Am. Chem. Soc.* **2006**, *128*, 4612. (b) Hwang, I.-W.; et al. *Chem.—Eur. J.* **2005**, *11*, 3753.

(5) (a) Ahn, T. K.; Yoon, Z. S.; Hwang, I.-W.; Lim, J. K.; Rhee, H.; Joo, T.; Sim, E.; Kim, S. K.; Aratani, N.; Osuka, A.; Kim, D. *J. Phys. Chem. B* **2005**, *109*, 11223. (b) Aratani, N.; Takagi, A.; Yanagawa, Y.; Matsumoto, T.; Kawai, T.; Yoon, Z. S.; Kim, D.; Osuka, A. *Chem.—Eur. J.* **2005**, *11*, 3389–3404. (c) Kim, Y. H.; Jeong, D. H.; Kim, D.; Jeoung, S. C.; Cho, H. S.; Kim, S. K.; Aratani, N.; Osuka, A. *J. Am. Chem. Soc.* **2001**, *123*, 76.

(6) (a) Ahn, T. K.; Kim, K. S.; Kim, D. Y.; Noh, S. B.; Aratani, N.; Ikeda, C.; Osuka, A.; Kim, D. *J. Am. Chem. Soc.* **2006**, *128*, 1700. (b) Kim, D.; Osuka, A. *J. Phys. Chem. A* **2003**, *107*, 8791. (c) Cho, H. S.; Jeong, D. H.; Cho, S.; Kim, D.; Matsuzaki, Y.; Tanaka, K.; Tsuda, A.; Osuka, A. *J. Am. Chem. Soc.* **2002**, *124*, 14642. (d) Tsuda, A.; Osuka, A. *Science* **2001**, *293*, 79.

(7) Ikeda, T.; Lintuluoto, J. M.; Aratani, N.; Yoon, Z. S.; Kim, D.; Osuka, A. *Eur. J. Org. Chem.* **2006**, 3193.

(8) (a) Tsuda, A.; Nakamura, Y.; Osuka, A. *Chem. Commun.* **2003**, 1096. (b) Tsuda, A.; Furuta, H.; Osuka, A. *J. Am. Chem. Soc.* **2001**, *123*, 10304.

(9) Yoon, M.-C.; Noh, S. B.; Tsuda, A.; Nakamura, Y.; Osuka, A.; Kim, D. *J. Am. Chem. Soc.* **2007**, *129*, 10080.

(10) Ikeda, T.; Aratani, N.; Easwaramoorthi, S.; Kim, D.; Osuka, A. *Org. Lett.* **2009**, *11*, 3080.

(11) Sheik-Bahae, M.; Said, A. A.; Wei, T.-H.; Hagan, D. G.; Van Stryland, E. W. *IEEE J. Quantum Electron.* **1990**, *26*, 760.

(12) Kim, O. K.; Lee, K. S.; Woo, H. Y.; Kim, K. S.; He, G. S.; Swiatkiewicz, J.; Prasad, P. N. *Chem. Mater.* **2000**, *12*, 284.

(13) *Surface Xplorer*; Ultrafast Systems LLC: Sarasota, FL.

(14) Frisch, M. J.; Trucks, G. W.; Schlegel, H. B.; Scuseria, G. E.; Robb, M. A.; Cheeseman, J. R.; Montgomery, J. A., Jr.; Vreven, T.; Kudin, K. N.; Burant, J. C.; Millam, J. M.; Iyengar, S. S.; Tomasi, J.; Barone, V.; Mennucci, B.; Cossi, M.; Scalmani, G.; Rega, N.; Petersson, G. A.; Nakatsuji, H.; Hada, M.; Ehara, M.; Toyota, K.; Fukuda, R.; Hasegawa, J.; Ishida, M.; Nakajima, T.; Honda, Y.; Kitao, O.; Nakai, H.; Klene, M.; Li, X.; Knox, J. E.; Hratchian, H. P.; Cross, J. B.; Bakken, V.; Adamo, C.; Jaramillo, J.; Gomperts, R.; Stratmann, R. E.; Yazyev, O.; Austin, A. J.; Cammi, R.; Pomelli, C.; Ochterski, J. W.; Ayala, P. Y.; Morokuma, K.; Voth, G. A.; Salvador, P.; Dannenberg, J. J.; Zakrzewski, V. G.; Dapprich, S.; Daniels, A. D.; Strain, M. C.; Farkas, O.; Malick, D. K.; Rabuck, A. D.; Raghavachari, K.; Foresman, J. B.; Ortiz, J. V.; Cui, Q.; Baboul, A. G.; Clifford, S.; Cioslowski, J.; Stefanov, B. B.; Liu, G.; Liashenko, A.; Piskorz, P.; Komaromi, I.; Martin, R. L.; Fox, D. J.; Keith, T.; Al-Laham, M. A.; Peng, C. Y.; Nanayakkara, A.; Challacombe, M.; Gill, P. M. W.; Johnson, B.; Chen, W.; Wong, M. W.; Gonzalez, C.; Pople, J. A. *Gaussian 03*, revision C.02; Gaussian, Inc.: Wallingford, CT, 2004.

(15) **FD2**: $C_{142}H_{175}N_8O_{11}Zn_2$, $Mw = 5832.35$, triclinic, space group $P$-1 (no. 2), $a = 11.169(3)$, $b = 23.483(7)$, $c = 26.382(7)$ Å, $\alpha = 64.175(10)$, $\beta = 85.946(9)$, $\gamma = 88.320(10)°$, $V = 6213(3)$ Å$^3$, $Z = 2$, $T = 90(2)$ K, $D_{calcd} = 1.238$ g cm$^{-3}$, $R_1 = 0.0603$ ($I > 2\sigma(I)$), $R_w = 0.1575$ (all data), GOF = 1.028.

(16) (a) Nakamura, Y.; Jang, S. Y.; Tanaka, T.; Aratani, N.; Lim, J. M.; Kim, K. S.; Kim, D.; Osuka, A. *Chem.—Eur. J.* **2008**, *14*, 8279. (b) Drobizhev, M.; Stepanenko, Y.; Dzenis, Y.; Karotki, A.; Rebane, A.; Taylor, P. N.; Anderson, H. L. *J. Am. Chem. Soc.* **2004**, *126*, 15352. (c) Drobizhev, M.; Stepanenko, Y.; Rebane, A.; Wilson, C. J.; Screen, T. E. O.; Anderson, H. L. *J. Am. Chem. Soc.* **2006**, *128*, 12432. (d) Hisaki, I.; Hiroto, S.; Kim, K. S.; Noh, S. B.; Kim, D.; Shinokubo, H.; Osuka, A. *Angew. Chem.* **2007**, *46*, 5125.

JP1022696